

INFLUENCE OF MICROSTRUCTURE ON DEBONDING AT THE FIBER/MATRIX INTERFACE IN FIBER-REINFORCED POLYMERS UNDER TENSILE LOADING

Luca Di Stasio^{1,2}

Supervisors: Janis Varna¹, Zoubir Ayadi²

¹Division of Materials Science, Luleå University of Technology, Luleå, Sweden

²EEIGM & IJL, Université de Lorraine, Nancy, France

Luleå (SE) - December 13, 2019



Outline

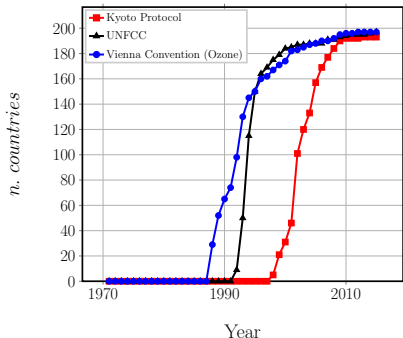
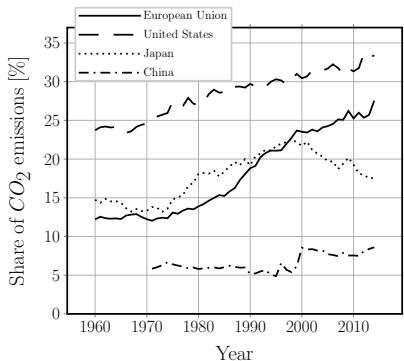
- ➔ Introduction
- ➔ Modeling
- ➔ Convergence
- ➔ Debond Initiation
- ➔ Debond Propagation
- ➔ Moving Forward

Introduction Modeling Convergence Debond Initiation Debond Propagation Moving Forward
Challenges of the transport sector The Thin-ply "Advantage" Micromechanics of Initiation

INTRODUCTION

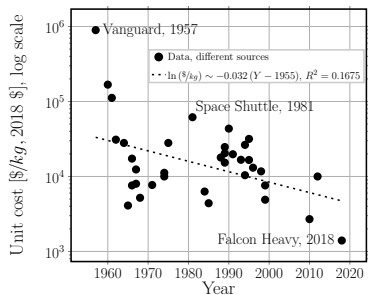
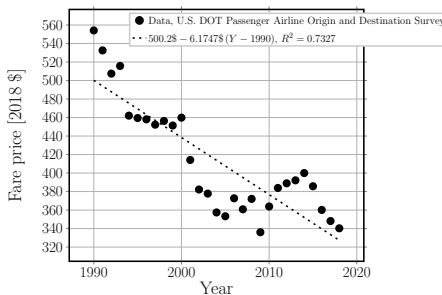
Challenges of the transport sector

- Institutional and popular pressure to reduce CO_2 emissions



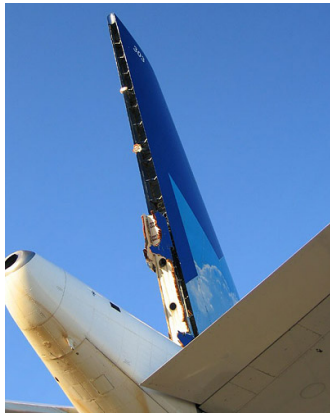
Challenges of the transport sector

→ Downward pressure on prices

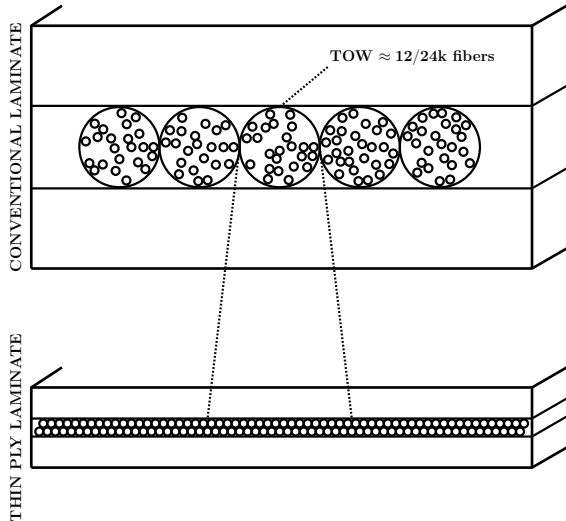


Challenges of the transport sector

- Strict requirements of safety and crashworthiness

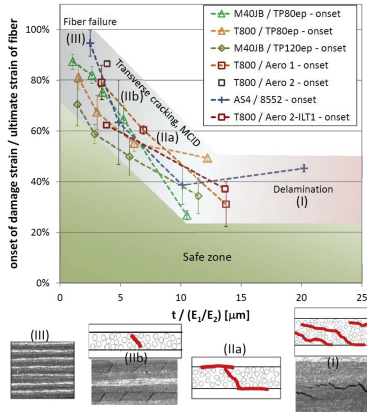


The Thin-ply "Advantage": new material



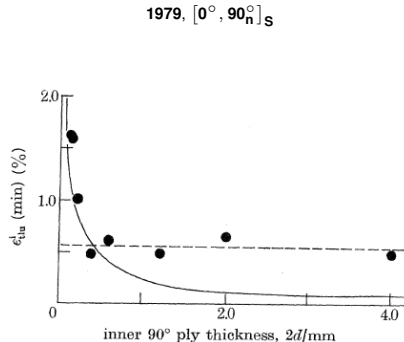
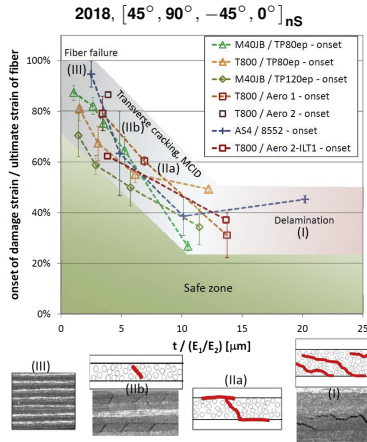
The Thin-ply "Advantage": new material

2018, $[45^\circ, 90^\circ, -45^\circ, 0^\circ]_{ns}$



Cugnoni et al., Compos. Sci. Technol. **168**, 2018.

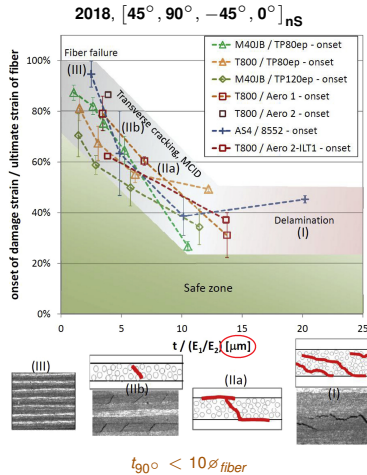
The Thin-ply "Advantage": new material, old result



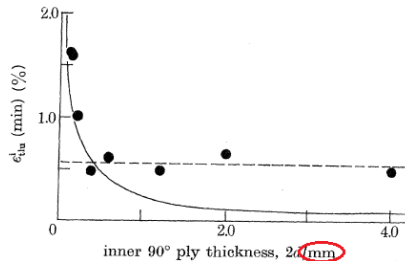
Cugnoni et al., Compos. Sci. Technol. **168**, 2018.

Bailey et al., P. Roy. Soc. A-Math. Phy. **366** (1727), 1979.

The Thin-ply "Advantage": new material, old result?

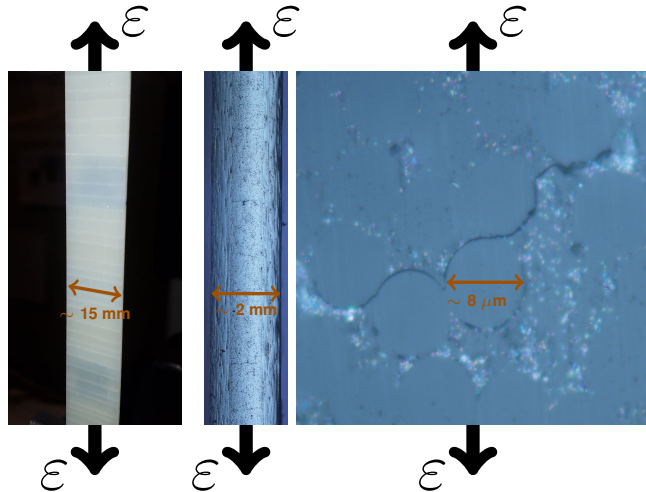


Cugnoni et al., Compos. Sci. Technol. **168**, 2018.



Bailey et al., P. Roy. Soc. A-Math. Phy. **366** (1727), 1979.

Micromechanics of Initiation



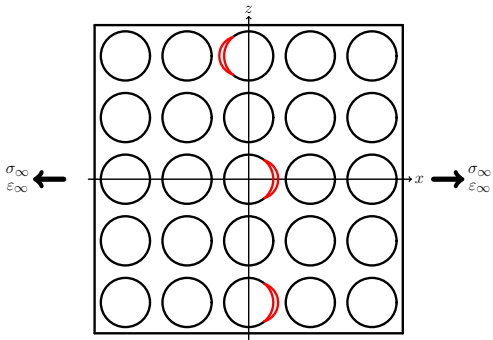
Left:
front view of $[0, 90]_S$,
visual inspection.

Center:
edge view of $[0, 90]_S$,
optical microscope.

Right:
edge view of $[0, 90]_S$,
optical microscope.

Micromechanics of Initiation

Stage 1: isolated debonds



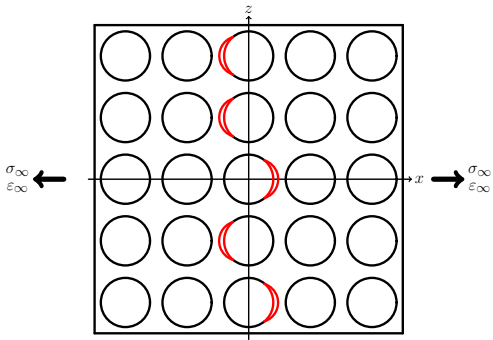
Bailey et al., P. Roy. Soc. A-Math. Phy. **366** (1727), 1979.

Bailey et al., J. Mater. Sci. **16** (3), 1981.

Zhang et al., Compos. Part A-Appl. S. **28** (4), 1997.

Micromechanics of Initiation

Stage 2: consecutive debonds



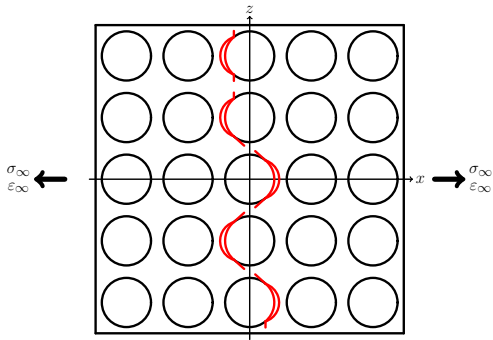
Bailey et al., P. Roy. Soc. A-Math. Phy. **366** (1727), 1979.

Bailey et al., J. Mater. Sci. **16** (3), 1981.

Zhang et al., Compos. Part A-Appl. S. **28** (4), 1997.

Micromechanics of Initiation

Stage 3: kinking



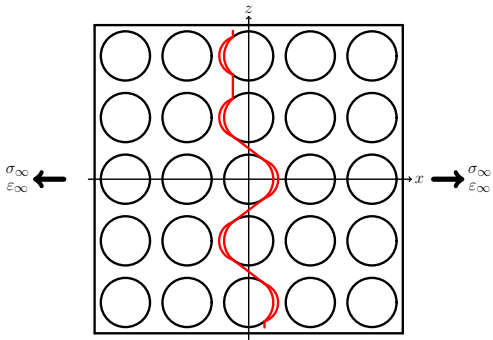
Bailey et al., P. Roy. Soc. A-Math. Phy. **366** (1727), 1979.

Bailey et al., J. Mater. Sci. **16** (3), 1981.

Zhang et al., Compos. Part A-Appl. S. **28** (4), 1997.

Micromechanics of Initiation

Stage 4: coalescence



Bailey et al., P. Roy. Soc. A-Math. Phy. **366** (1727), 1979.

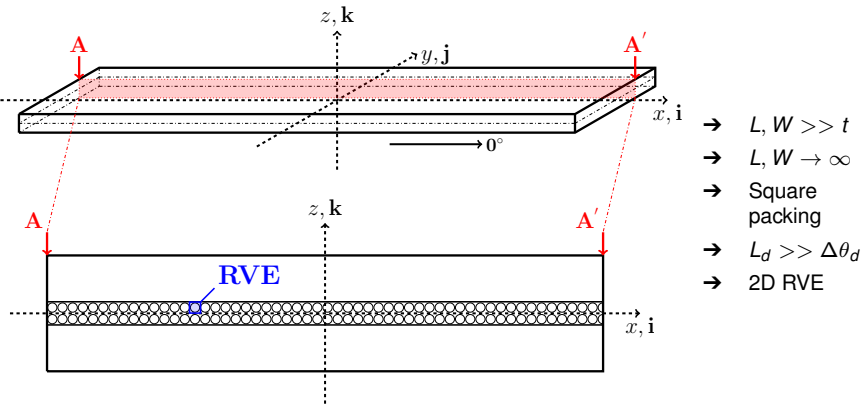
Bailey et al., J. Mater. Sci. **16** (3), 1981.

Zhang et al., Compos. Part A-Appl. S. **28** (4), 1997.

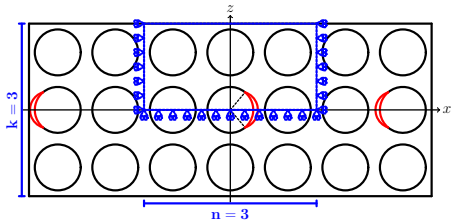
Introduction Modeling Convergence Debond Initiation Debond Propagation Moving Forward
Geometry Representative Volume Elements Equivalent boundary conditions Assumptions Solution

MODELING

Geometry

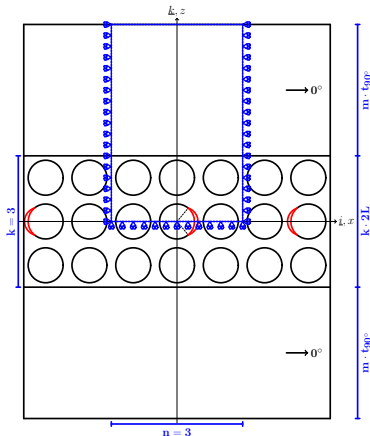


Representative Volume Elements



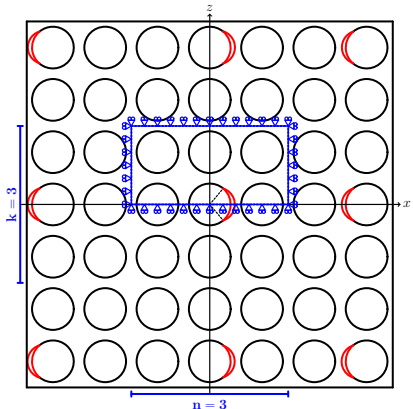
$n \times k - \text{free}$

$n \times k - H$



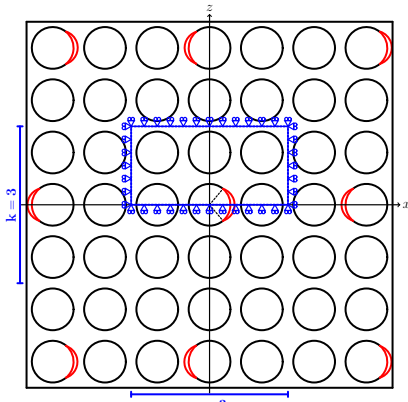
$n \times k - m \cdot t_{90^\circ}$

Representative Volume Elements



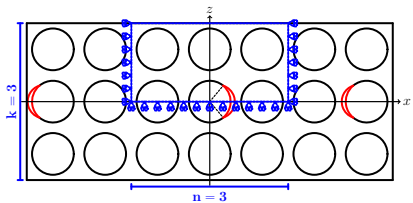
$n \times k - \text{symm (coupling)}$

$n \times k - \text{coupling} + H$



$n \times k - \text{asymm}$

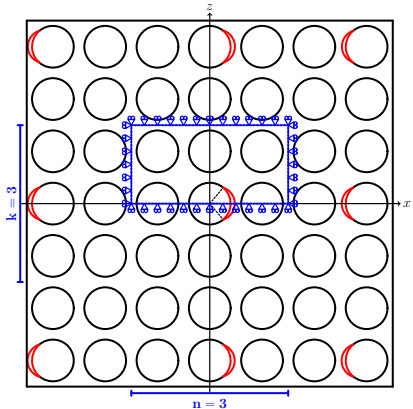
Equivalent boundary conditions: linear horizontal displacement (H)



$$u_x(x, h) = \bar{\varepsilon}_x x$$

$$n \times k - H$$

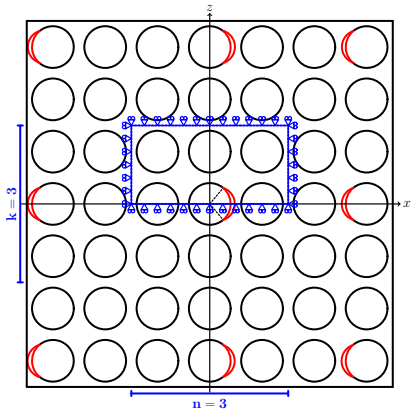
Equivalent boundary conditions: symmetric coupling



$$u_z(x, h) = \bar{u}_z(x, h)$$

$n \times k - \text{symm (coupling)}$

Equivalent boundary conditions: coupling + H



$$u_z(x, h) = \bar{u}_z(x, h)$$

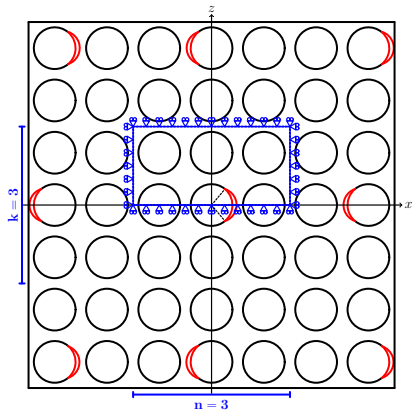
$$u_x(x, h) = \bar{\varepsilon}_x x$$

$n \times k - \text{coupling} + H$

Equivalent boundary conditions: anti-symmetric coupling

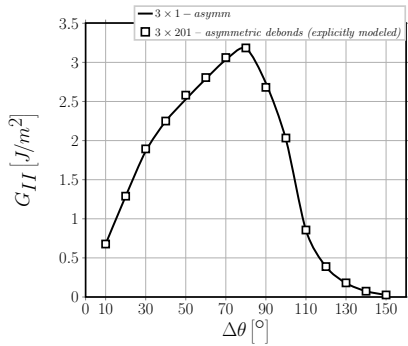
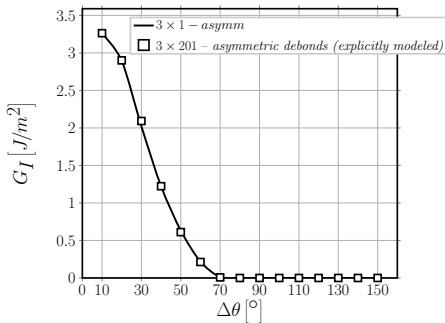
$$\begin{aligned} u_z(x, h) - u_z(0, h) = \\ - (u_z(-x, h) - u_z(0, h)) \end{aligned}$$

$$u_x(x, h) = -u_x(-x, h)$$

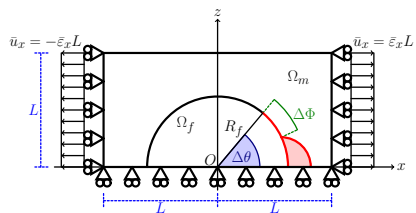


$n \times k - asymm$

Equivalent boundary conditions: validation



Assumptions

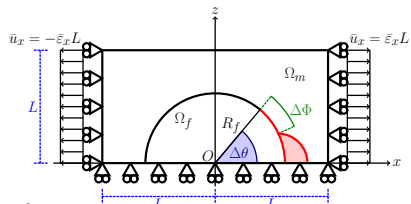


$$R_f = 1 \text{ } [\mu\text{m}] \quad L = \frac{R_f}{2} \sqrt{\frac{\pi}{V_f}}$$

- Linear elastic, homogeneous materials
- Concentric Cylinders Assembly with Self-Consistent Shear Model for UD
- Plane strain
- Frictionless contact interaction
- Symmetric w.r.t. x-axis
- Coupling of x-displacements on left and right side (repeating unit cell)
- Applied uniaxial tensile strain $\bar{\epsilon}_x = 1\%$
- $V_f = 60\%$

Material	V_f [%]	E_L [GPa]	E_T [GPa]	μ_{LT} [GPa]	ν_{LT} [-]	ν_{TT} [-]
Glass fiber	-	70.0	70.0	29.2	0.2	0.2
Epoxy	-	3.5	3.5	1.25	0.4	0.4
UD	60.0	43.442	13.714	4.315	0.273	0.465

Solution



in $\Omega_f, \Omega_m, \Omega_{UD}$:

$$\frac{\partial^2 \varepsilon_{xx}}{\partial z^2} + \frac{\partial^2 \varepsilon_{zz}}{\partial x^2} = \frac{\partial^2 \gamma_{zx}}{\partial x \partial z} \quad \text{for } 0^\circ \leq \alpha \leq \Delta\theta : \quad (\vec{u}_m(R_f, \alpha) - \vec{u}_f(R_f, \alpha)) \cdot \vec{n}_\alpha \geq 0$$

$$\varepsilon_y = \gamma_{xy} = \gamma_{yz} = 0 \quad \text{for } \Delta\theta \leq \alpha \leq 180^\circ :$$

$$\frac{\partial \sigma_{xx}}{\partial x} + \frac{\partial \tau_{zx}}{\partial z} = 0 \quad \vec{u}_m(R_f, \alpha) - \vec{u}_f(R_f, \alpha) = 0$$

$$\frac{\partial \tau_{zx}}{\partial x} + \frac{\partial \sigma_{zz}}{\partial z} = 0 \quad \sigma_{ij} = E_{ijkl} \varepsilon_{kl}$$

$$\sigma_{yy} = \nu (\sigma_{xx} + \sigma_{zz})$$

$\forall \Delta\theta \neq 0^\circ$

→ oscillating singularity

$$\sigma \sim r^{-\frac{1}{2}} \sin(\varepsilon \log r), \quad V_f \rightarrow 0$$

$$\varepsilon = \frac{1}{2\pi} \log \left(\frac{1-\beta}{1+\beta} \right)$$

$$\beta = \frac{\mu_2(\kappa_1 - 1) - \mu_1(\kappa_2 - 1)}{\mu_2(\kappa_1 + 1) + \mu_1(\kappa_2 + 1)}$$

→ receding contact

$$\rightarrow \frac{G(R_{f,2})}{G(R_{f,1})} = \frac{R_{f,2}}{R_{f,1}}, \quad \frac{G(\bar{v}_{x,2})}{G(\bar{v}_{x,1})} = \frac{\bar{v}_{x,2}^2}{\bar{v}_{x,1}^2}$$

→ FEM + LEFM (VCCT)

→ regular mesh of quadrilaterals at the crack tip:

- $AR \sim 1, \quad \delta = 0.05^\circ$

$\forall \Delta\theta$

→ 2nd order shape functions

Introduction Modeling Convergence Debond Initiation Debond Propagation Moving Forward

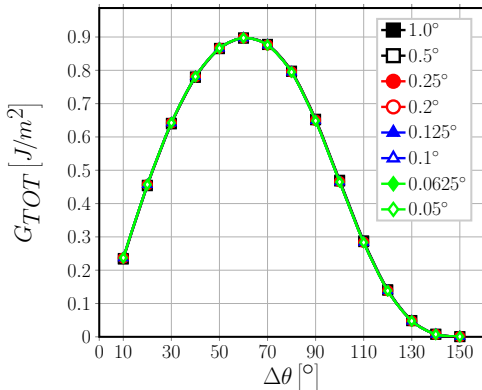
G_{TOT} G_I G_{II} Vectorial formulation of VCCT Asymptotic behavior Numerical convergence δ selection

CONVERGENCE

Introduction Modeling Convergence Debond Initiation Debond Propagation Moving Forward

G_{TOT} G_I G_{II} Vectorial formulation of VCCT Asymptotic behavior Numerical convergence δ selection

G_{TOT}

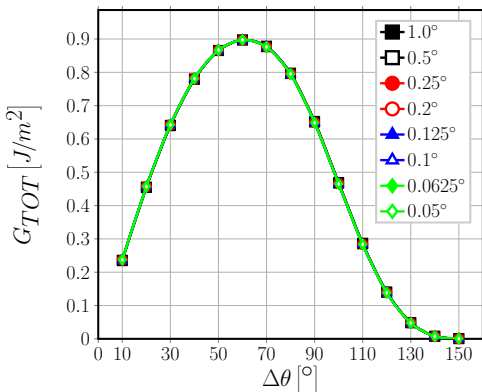


$\rightarrow 1 \times 1 - \text{free}, V_f = 0.1\%, 1^{\text{st}} \text{ order elements}$

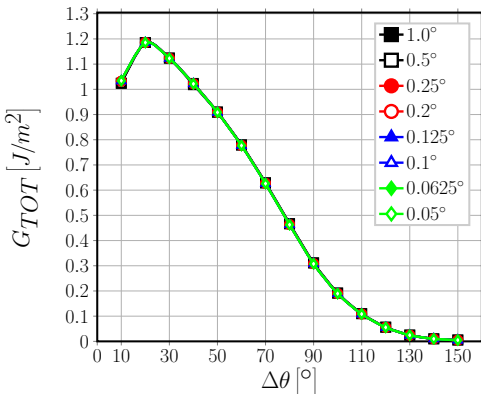
Introduction Modeling Convergence Debond Initiation Debond Propagation Moving Forward

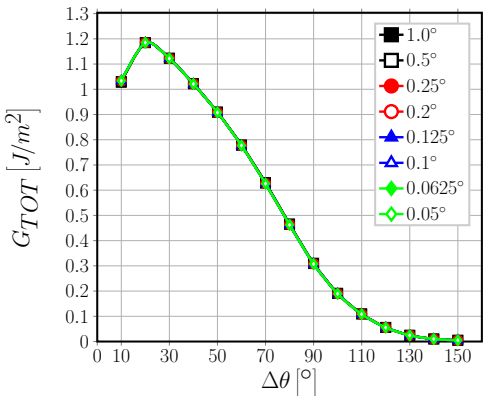
G_{TOT} G_I G_{II} Vectorial formulation of VCCT Asymptotic behavior Numerical convergence δ selection

G_{TOT}

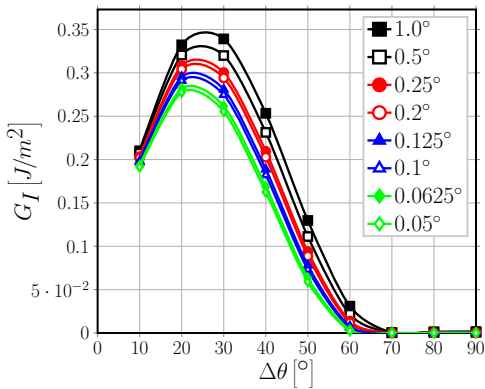


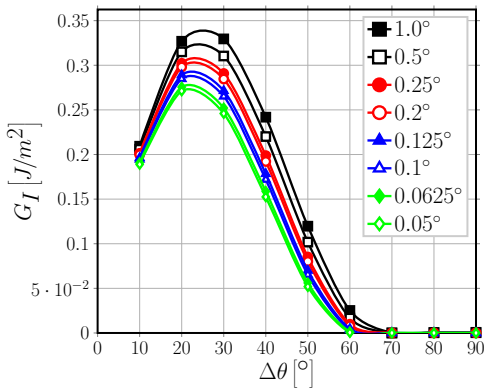
$\rightarrow 1 \times 1 - \text{free}, V_f = 0.1\%, 2^{\text{nd}} \text{ order elements}$

G_{TOT}  $\rightarrow 1 \times 1 - \text{free}, V_f = 40\%, 1^{st} \text{ order elements}$

G_{TOT} 

$\rightarrow 1 \times 1 - free, V_f = 40\%, 2^{nd} order elements$

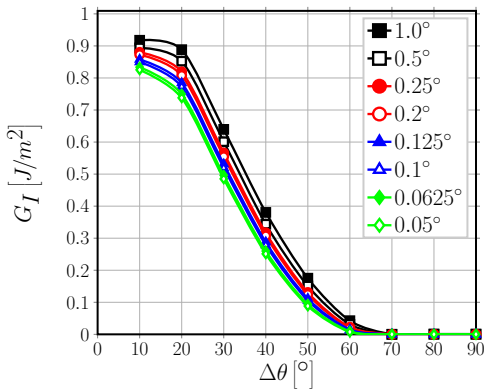
G_I  $\rightarrow 1 \times 1 - free, V_f = 0.1\%, 1^{st} \text{ order elements}$

G_I  $\rightarrow 1 \times 1 - free, V_f = 0.1\%, 2^{nd} order elements$

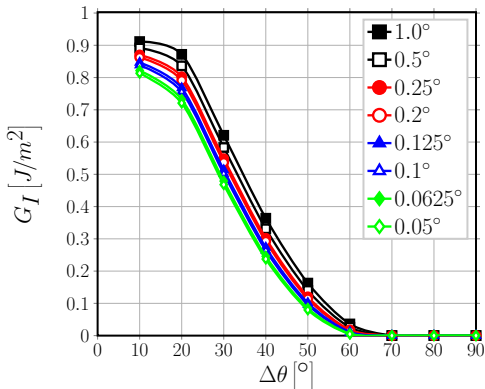
Introduction Modeling Convergence Debond Initiation Debond Propagation Moving Forward

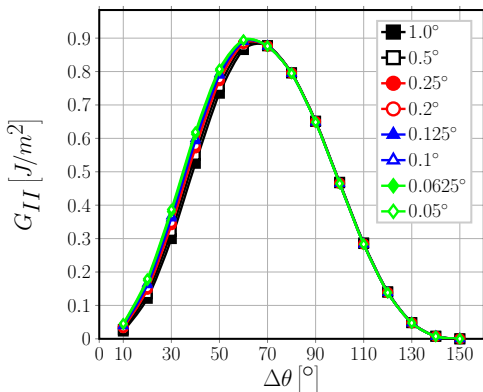
G_{TOT} G_I G_{II} Vectorial formulation of VCCT Asymptotic behavior Numerical convergence δ selection

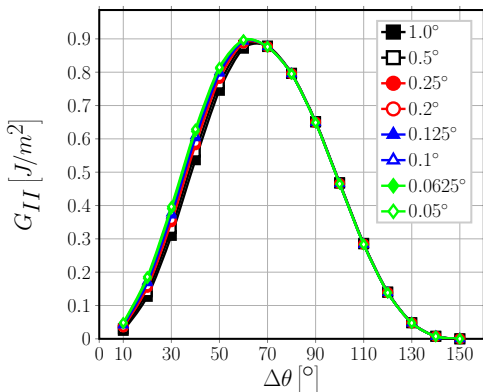
G_I

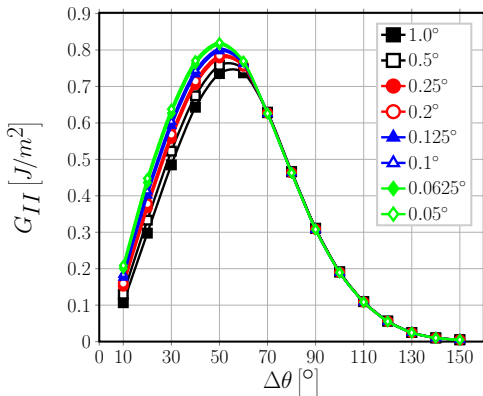


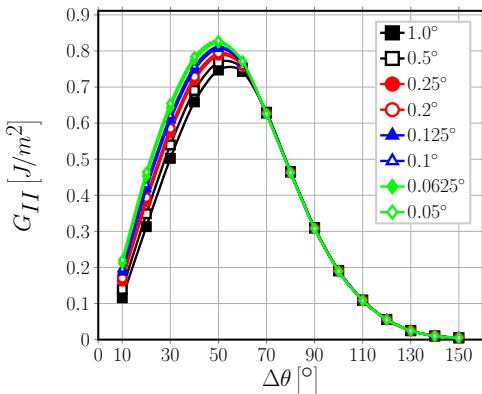
$\rightarrow 1 \times 1 - free, V_f = 40\%, 1^{st} order elements$

G_I  $\rightarrow 1 \times 1 - free, V_f = 40\%, 2^{nd} \text{ order elements}$

G_{II}  $\rightarrow 1 \times 1 - free, V_f = 0.1\%, 1^{st} \text{ order elements}$

G_{II}  $\rightarrow 1 \times 1 - free, V_f = 0.1\%, 2^{nd} order elements$

G_{II}  $\rightarrow 1 \times 1 - free, V_f = 40\%, 1^{st} order elements$

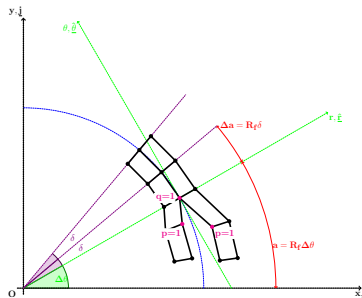
G_{II} 

$\rightarrow 1 \times 1 - \text{free}, V_f = 40\%, 2^{\text{nd}} \text{ order elements}$

Introduction Modeling Convergence Debond Initiation Debond Propagation Moving Forward

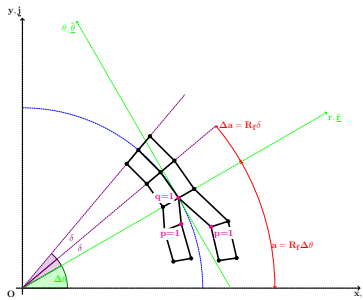
G_{TOT} G_I G_{II} Vectorial formulation of VCCT Asymptotic behavior Numerical convergence δ selection

Vectorial formulation of VCCT



$$G_{TOT} = \frac{1}{2R_f\delta} \sum_{p=1}^{m+1} \sum_{q=1}^{m+1} Tr \left(\underline{\underline{Q}}_{\underline{\underline{\delta}}=\Delta\theta} \underline{\underline{R}}_{\underline{\underline{\delta}}=\Delta\theta} \underline{\underline{K}}_{xy,q} \underline{\underline{u}}_{xy,q}^T, p \right) + \\ + \frac{1}{2R_f\delta} \sum_{p=1}^{m+1} \sum_{q=1}^{m+1} Tr \left(\underline{\underline{Q}}_{\underline{\underline{\delta}}=\Delta\theta} \underline{\underline{R}}_{\underline{\underline{\delta}}=\Delta\theta} \widetilde{\underline{\underline{F}}}_{xy,q} \underline{\underline{u}}_{xy,p}^T, R^T_{\underline{\underline{\delta}}=\Delta\theta} P^T_{\underline{\underline{\delta}}=\delta} T^T_{pq} \right)$$

Vectorial formulation of VCCT



$$\underline{G} = \begin{bmatrix} G_I \\ G_{II} \end{bmatrix} = \frac{1}{2R_f\delta} \sum_{p=1}^{m+1} \sum_{q=1}^{m+1} Diag \left(\underline{\underline{Q}}_{\underline{\underline{\delta}}} \underline{\underline{R}}_{\underline{\underline{\Delta\theta}}} \underline{\underline{K}}_{\underline{\underline{xy}},q} \underline{u}_{xy,q} \underline{u}_{xy,p}^T \underline{\underline{R}}_{\underline{\underline{\Delta\theta}}}^T \underline{\underline{P}}_{\underline{\underline{\delta}}}^T \underline{\underline{T}}_{\underline{\underline{pq}}}^T \right) + \\ + \frac{1}{2R_f\delta} \sum_{p=1}^{m+1} \sum_{q=1}^{m+1} Diag \left(\underline{\underline{Q}}_{\underline{\underline{\delta}}} \underline{\underline{R}}_{\underline{\underline{\Delta\theta}}} \widetilde{\underline{\underline{K}}}_{\underline{\underline{N}},q} \underline{u}_N \underline{u}_{xy,p}^T \underline{\underline{R}}_{\underline{\underline{\Delta\theta}}}^T \underline{\underline{P}}_{\underline{\underline{\delta}}}^T \underline{\underline{T}}_{\underline{\underline{pq}}}^T \right)$$

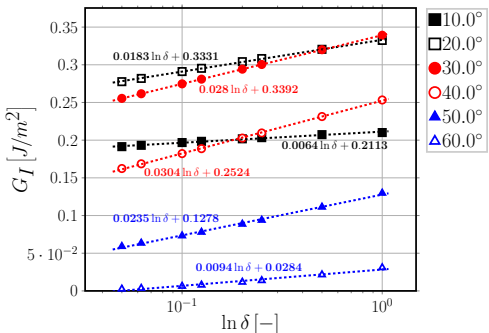
Asymptotic behavior

$$\frac{\partial \underline{G}}{\partial \delta} = \frac{1}{\delta} \underline{G} + \frac{1}{2R_f \delta} (\dots)$$

$$u(\delta) \sim \sqrt{\delta} (\sin, \cos)(\epsilon \log \delta) \quad \text{with} \quad \epsilon = \frac{1}{2\pi} \log \left(\frac{1-\beta}{1+\beta} \right)$$

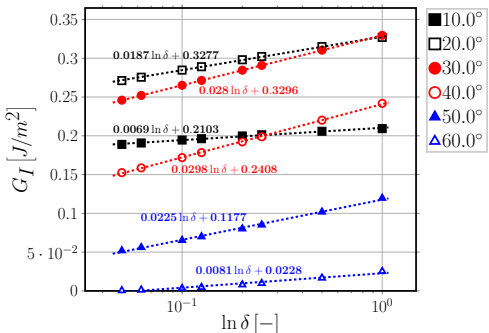
$$\lim_{\delta \rightarrow 0} \frac{\partial \underline{G}}{\partial \delta} \sim \frac{1}{\delta} \xrightarrow{\int d\delta} \lim_{\delta \rightarrow 0} \underline{G} \sim \underline{A} \log(\delta) + \underline{B}.$$

Numerical convergence: G_I



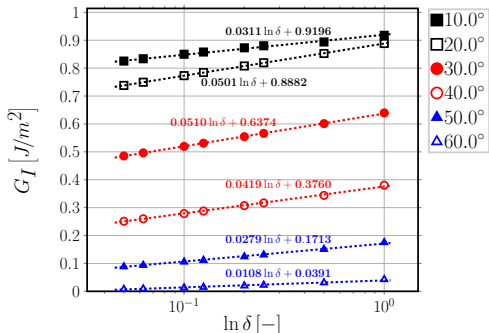
→ $1 \times 1 - free$, $V_f = 0.1\%$, 1st order elements

Numerical convergence: G_I



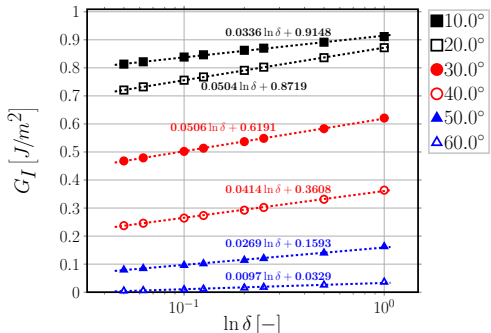
$\rightarrow 1 \times 1 - free, V_f = 0.1\%, 2^{nd} order elements$

Numerical convergence: G_I



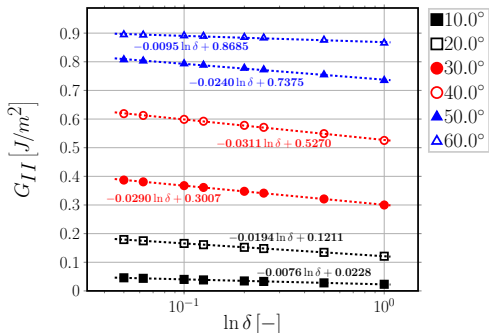
$\rightarrow 1 \times 1 - free, V_f = 40\%, 1^{st} order elements$

Numerical convergence: G_I



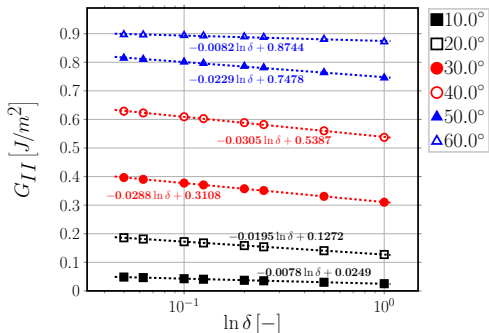
→ $1 \times 1 - free$, $V_f = 40\%$, 2nd order elements

Numerical convergence: G_{II}



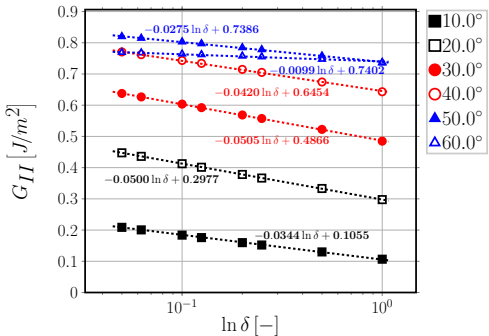
→ $1 \times 1 - free$, $V_f = 0.1\%$, 1st order elements

Numerical convergence: G_{II}



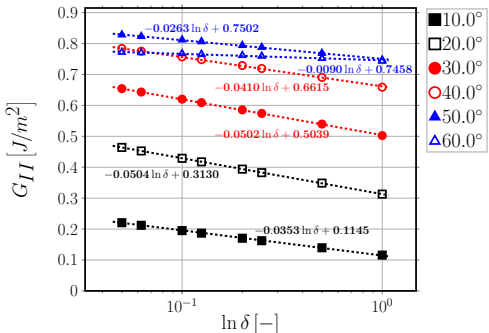
→ $1 \times 1 - \text{free}$, $V_f = 0.1\%$, 2nd order elements

Numerical convergence: G_{II}



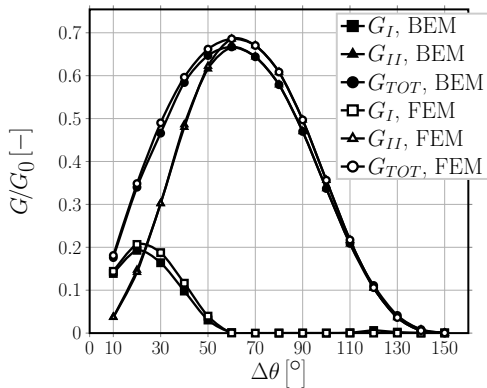
→ $1 \times 1 - free$, $V_f = 40\%$, 1st order elements

Numerical convergence: G_{II}



→ $1 \times 1 - \text{free}$, $V_f = 40\%$, 2nd order elements

δ selection

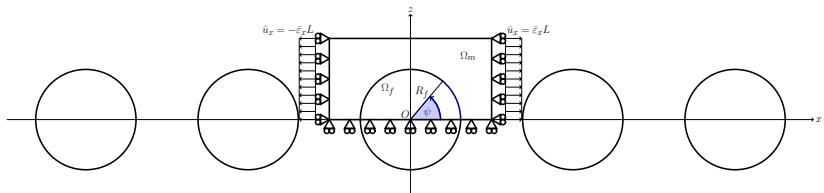
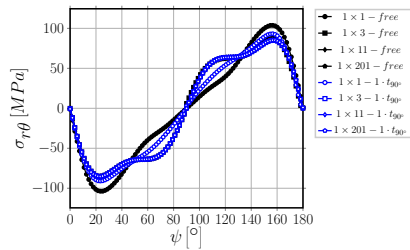
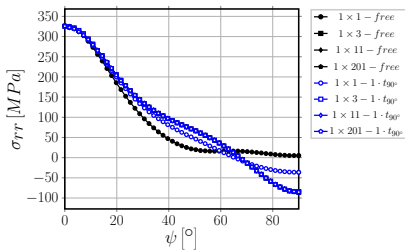


$\rightarrow 1 \times 1 - free$, $V_f = 0.01\%$, 2nd order elements, $\delta = 0.05^\circ$

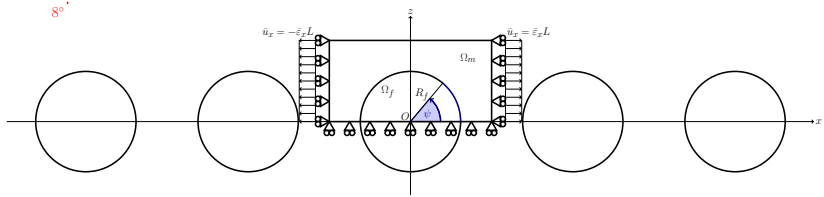
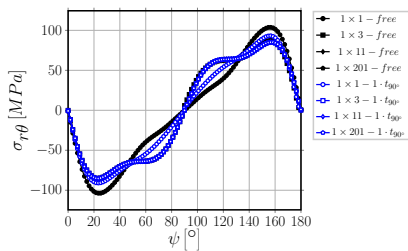
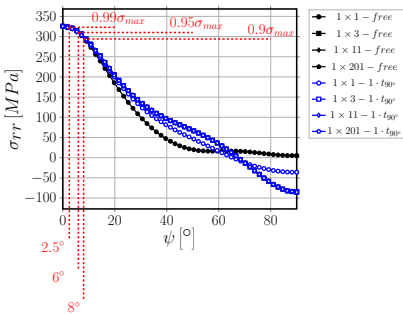
Introduction Modeling Convergence Debond Initiation Debond Propagation Moving Forward
 σ_{rr} vs $\tau_{r\theta}$ σ_{LHS} σ_{vM} σ_I Observations

DEBOND INITIATION

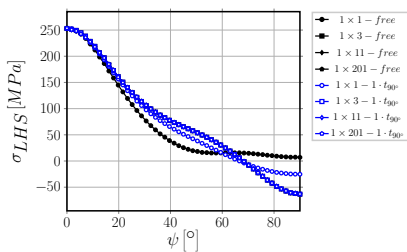
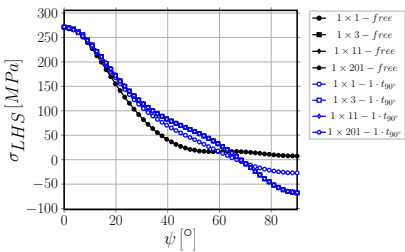
σ_{rr} vs $\tau_{r\theta}$: radial stress vs tangential shear at the interface



σ_{rr} vs $\tau_{r\theta}$: radial stress vs tangential shear at the interface

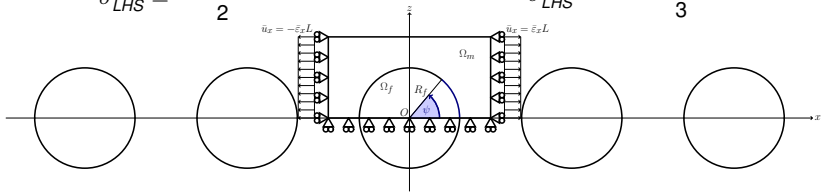


σ_{LHS} : local hydrostatic stress at the interface

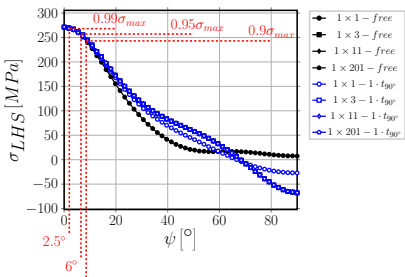


$$\sigma_{LHS}^{2D} = \frac{\sigma_{rr} + \sigma_{\theta\theta}}{2}$$

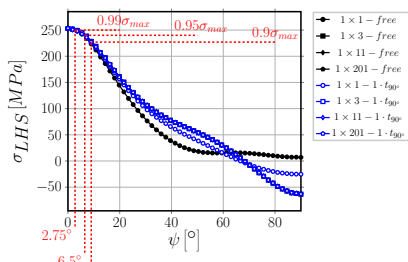
$$\sigma_{LHS}^{3D} = \frac{\sigma_{rr} + \sigma_{\theta\theta} + \sigma_{yy}}{3}$$



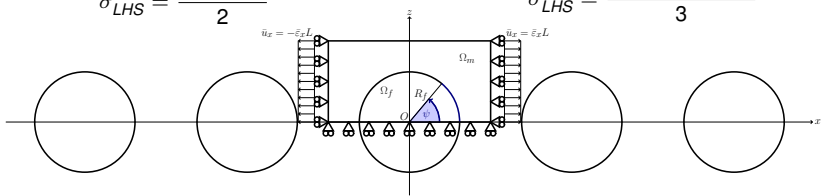
σ_{LHS} : local hydrostatic stress at the interface



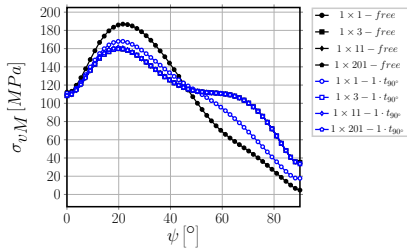
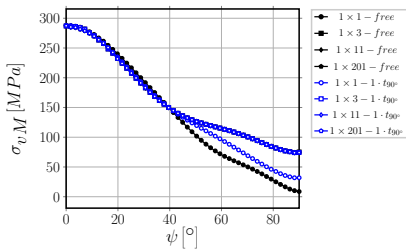
$$\sigma_{LHS}^{2D} = \frac{\sigma_{rr} + \sigma_{\theta\theta}}{2}$$



$$\sigma_{LHS}^{3D} = \frac{\sigma_{rr} + \sigma_{\theta\theta} + \sigma_{yy}}{3}$$

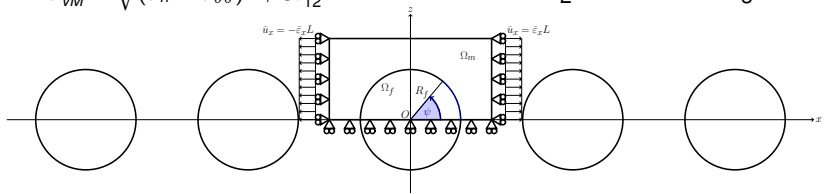


σ_{vM} : von Mises stress at the interface

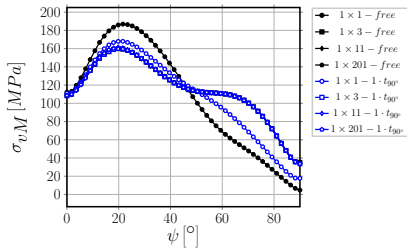
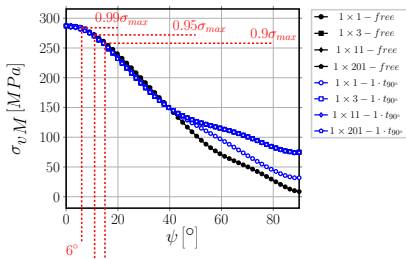


$$\sigma_{vM}^{2D} = \sqrt{(\sigma_{rr} - \sigma_{\theta\theta})^2 + 3\tau_{12}^2}$$

$$\sigma_{LHS}^{3D} = \frac{3}{2} s_{ij} s_{ij} \quad s_{ij} = \sigma_{jj} - \frac{1}{3} \sigma_{kk} \delta_{ij}$$

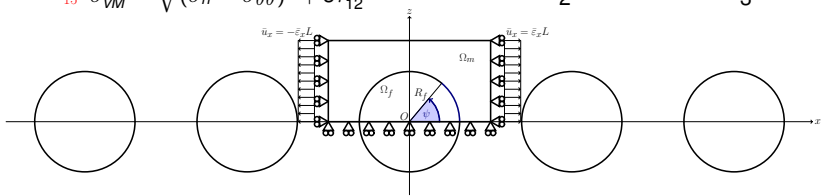


σ_{vM} : von Mises stress at the interface

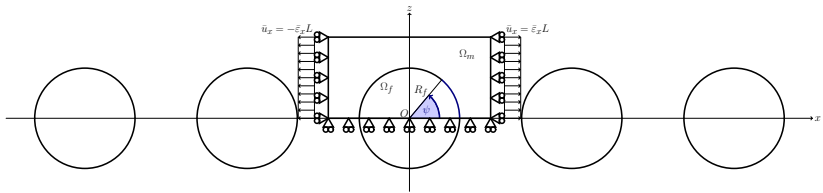
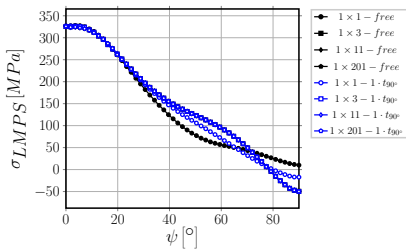
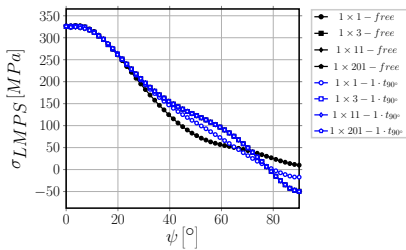


$$\sigma_{vM}^{2D} = \sqrt{(\sigma_{rr} - \sigma_{\theta\theta})^2 + 3\tau_{12}^2}$$

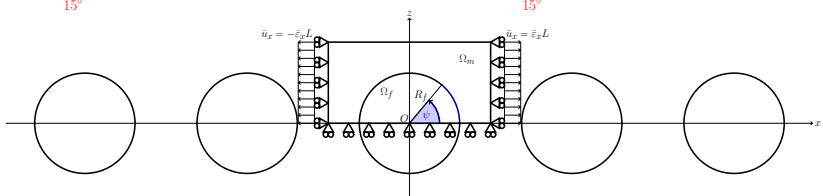
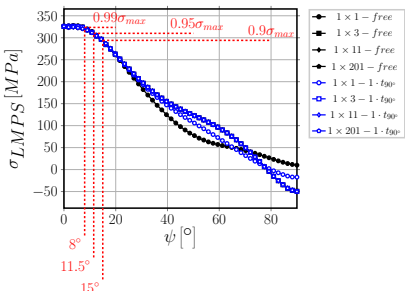
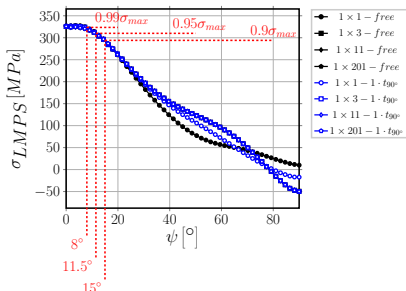
$$\sigma_{LHS}^{3D} = \frac{3}{2} s_{ij} s_{ij} \quad s_{ij} = \sigma_{ij} - \frac{1}{3} \sigma_{kk} \delta_{ij}$$



σ_I : maximum principal stress at the interface



σ_I : maximum principal stress at the interface



Observations

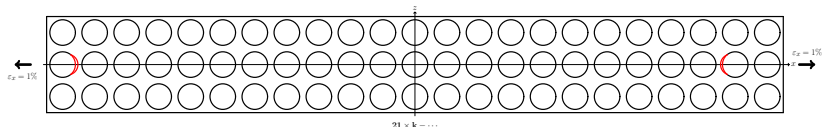
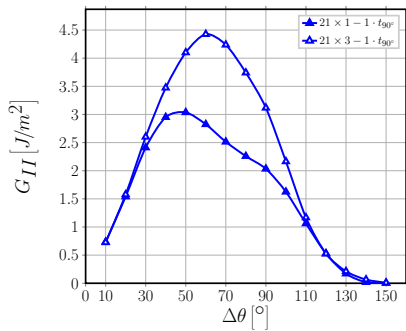
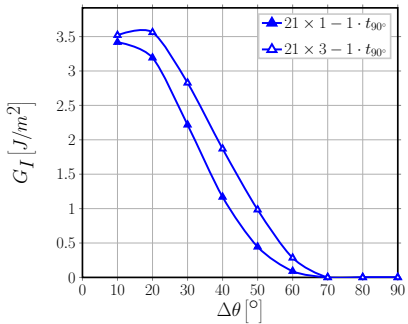
- For all stresses analyzed, no significant difference is present between the different RUCs for $\psi \leq 10^\circ$;
- for all stresses analyzed, no difference can be observed by increasing k when $k \geq 3$;
- for all stresses analyzed, no difference can be observed between $1 \times k - \text{free}$ and $1 \times k - 1 \cdot t_{90^\circ}$ for $k \geq 3$;
- σ_{rr} , $\sigma_{LHS,2D}$, $\sigma_{LHS,3D}$, $\sigma_{vM,2D}$, $\sigma_{LMPS,2D}$ and $\sigma_{LMPS,3D}$ all reach their peak value at 0° and 180° and decrease to 99% the peak value between 2° and 8° , to 95% the peak value between 6° and 12° and to 90% the peak value between 8° and 15° from the occurrence of the maximum.

It seems reasonable to conclude that...

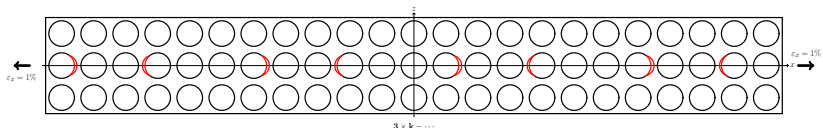
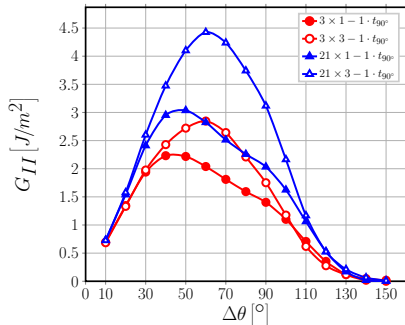
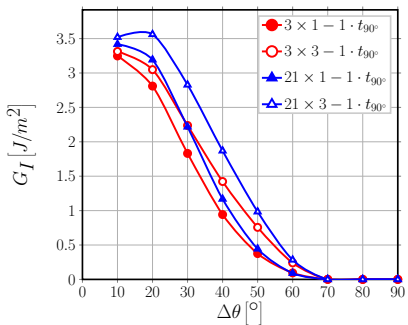
...a stress-based criterion would predict, irrespectively of the specific criterion chosen, the onset of an interface crack at 0° or 180° with an initial size at least comprised in the range $2^\circ - 8^\circ$ (1% margin) and likely in the range $6^\circ - 12^\circ$ (5% margin). Thus, no evident effect of 90° or 0° layer thickness can be observed.

DEBOND PROPAGATION

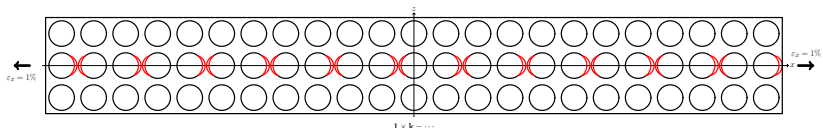
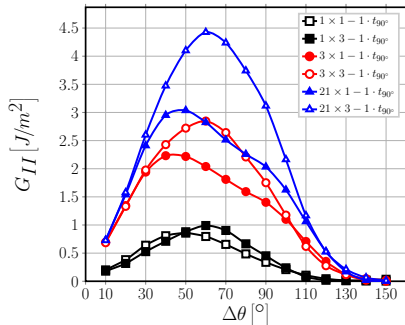
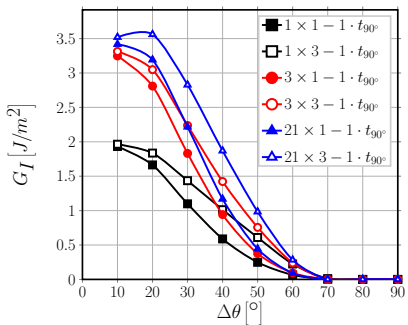
Interaction of Debonds: Crack Shielding



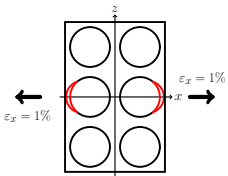
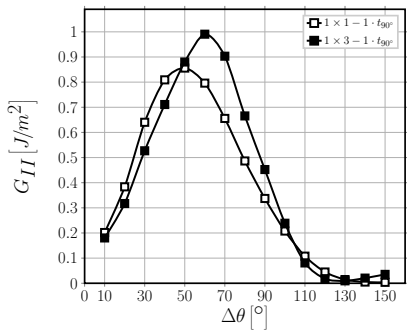
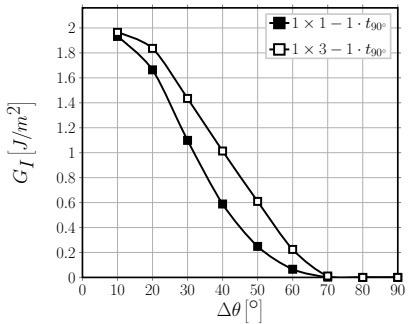
Interaction of Debonds: Crack Shielding



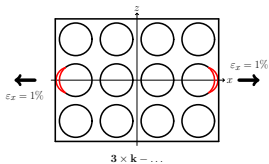
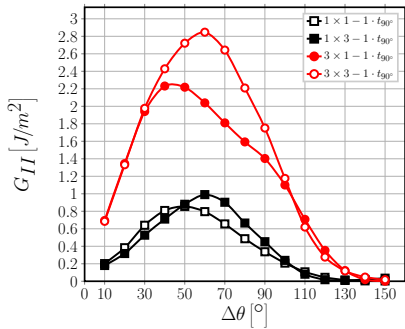
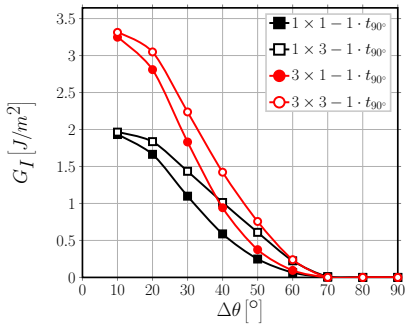
Interaction of Debonds: Crack Shielding



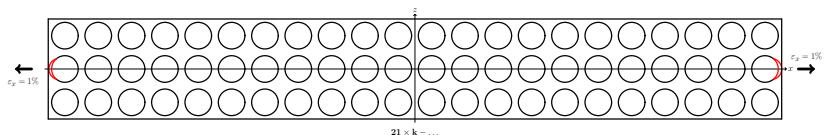
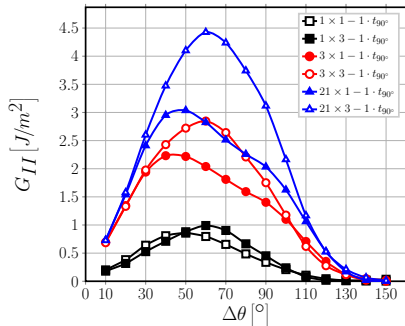
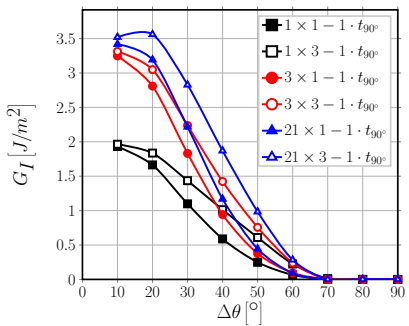
Interaction of Debonds: Strain Magnification



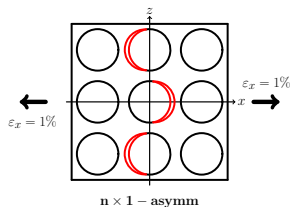
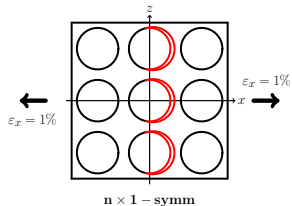
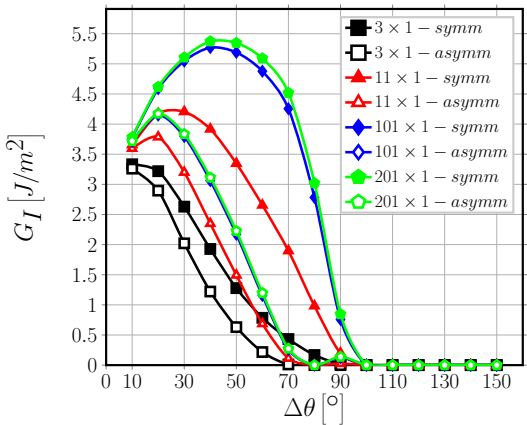
Interaction of Debonds: Strain Magnification



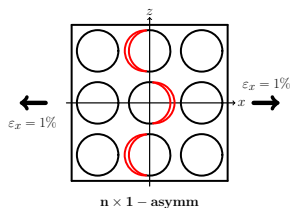
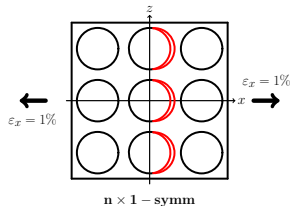
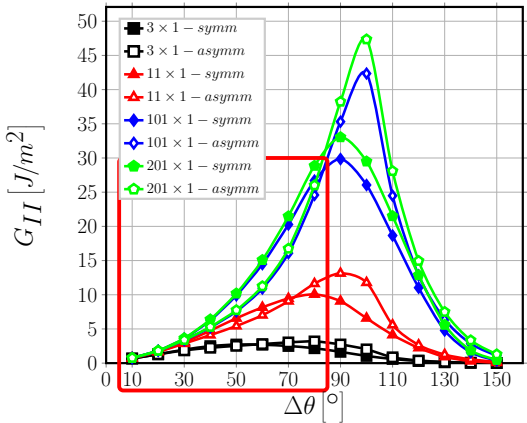
Interaction of Debonds: Strain Magnification



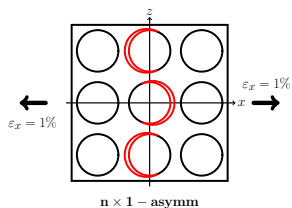
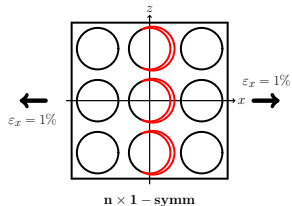
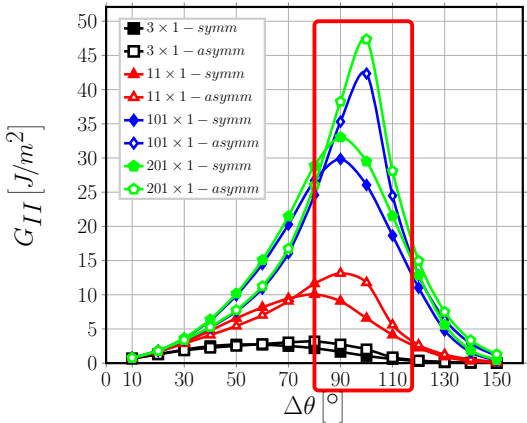
Consecutive Debonds: Mode I



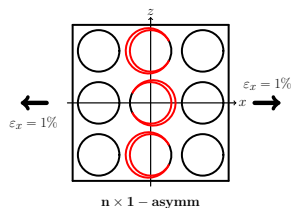
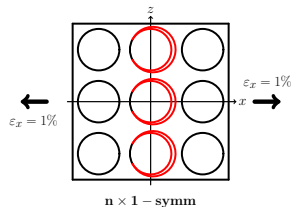
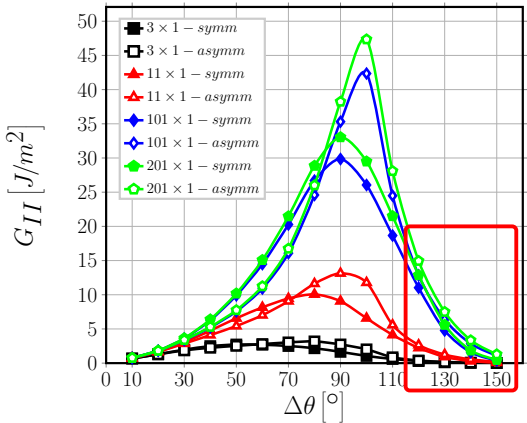
Consecutive Debonds: Mode II



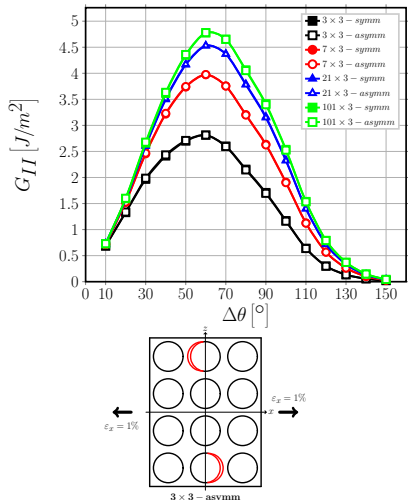
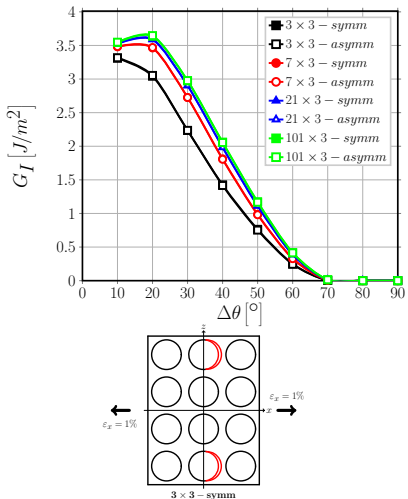
Consecutive Debonds: Mode II



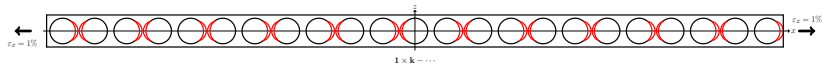
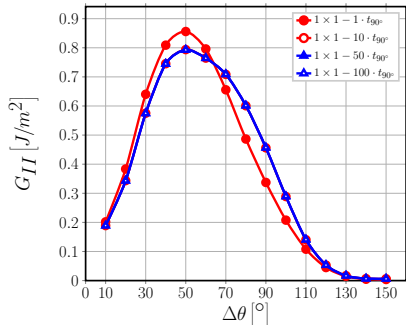
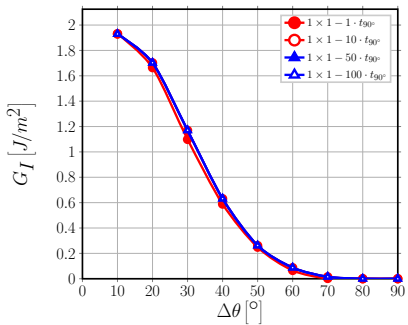
Consecutive Debonds: Mode II



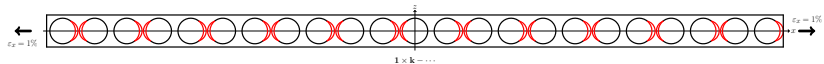
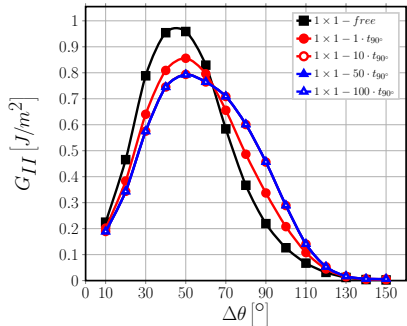
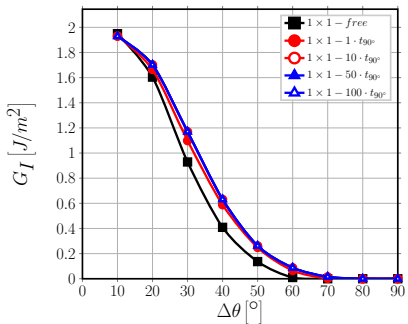
Non-Consecutive Debonds



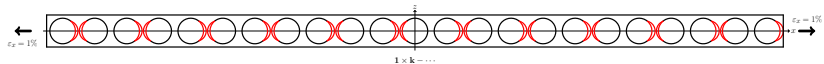
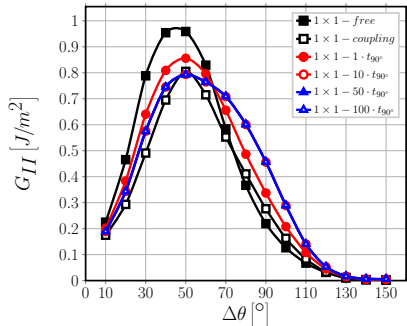
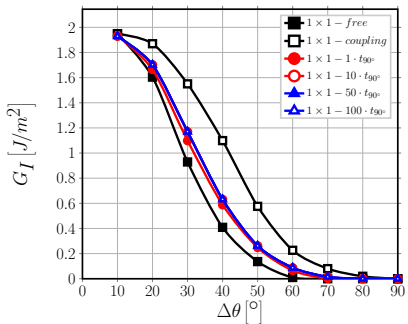
Effect of 0° ply thickness



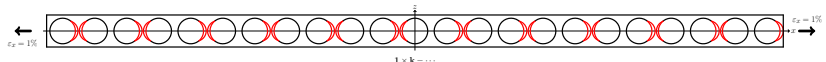
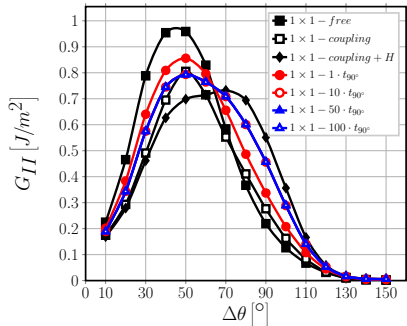
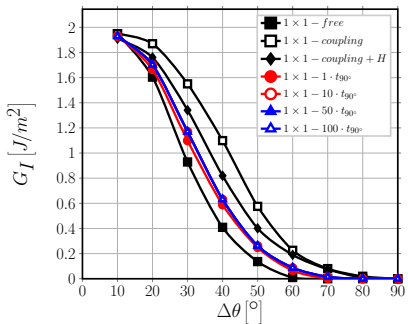
Effect of 0° ply thickness



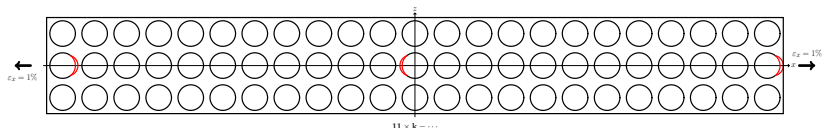
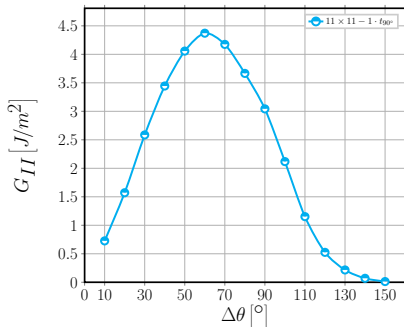
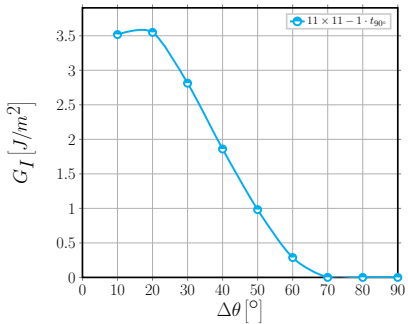
Effect of 0° ply thickness



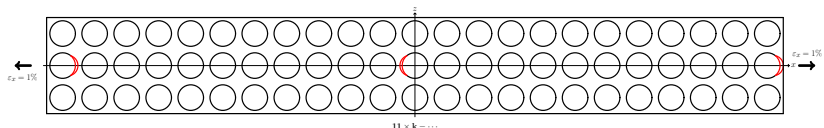
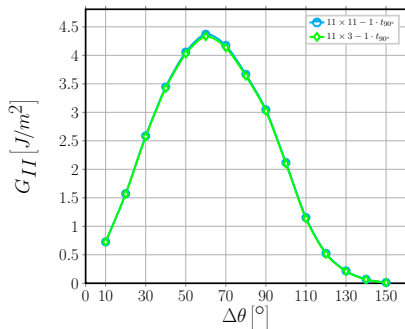
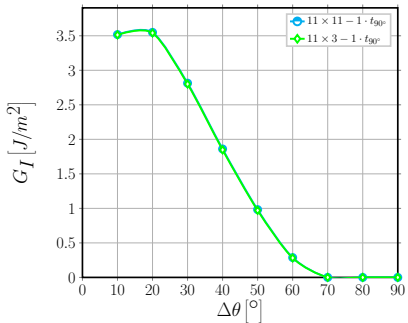
Effect of 0° ply thickness



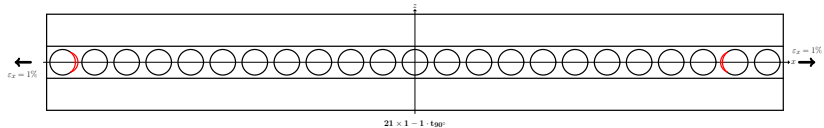
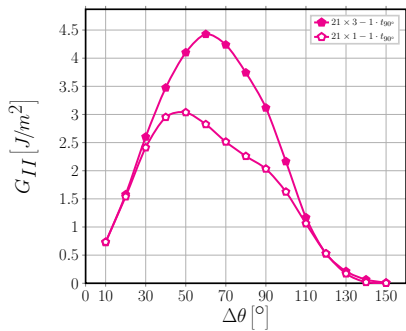
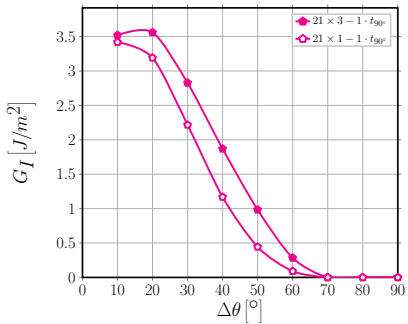
Effect of 90° ply thickness



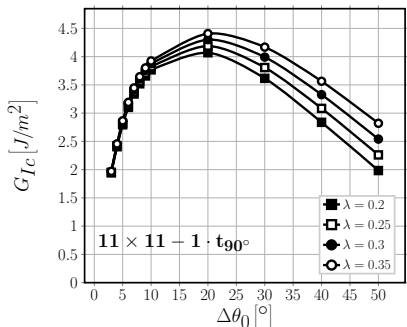
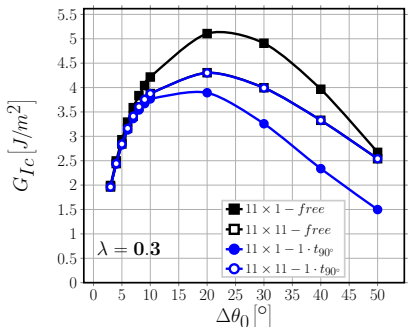
Effect of 90° ply thickness



Effect of 90° ply thickness



Estimation of G_{Ic}

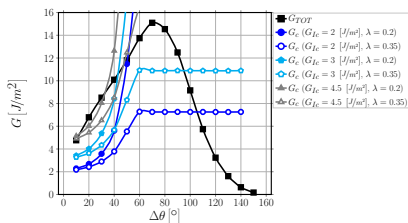


$$G_{Ic} = \frac{G_c}{1 + \tan^2((1 - \lambda) \Psi_G)} \Big|_{G_c=G_{TOT}(\Delta\theta_0)}, \quad \Psi_G = \tan^{-1} \left(\sqrt{\frac{G_{II}}{G_I}} \right) \Big|_{\Delta\theta_0}$$

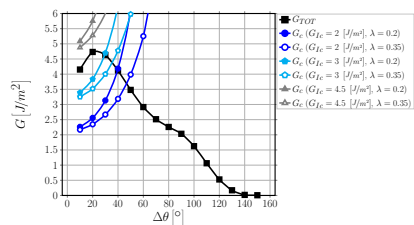
$G_{Ic} \in [2, 4.5] \text{ J/m}^2$ with $R_f = 1 \mu\text{m}$, $\bar{\varepsilon}_x = 1\%$, $G_{Ic} \in [3.2, 7.2] \text{ J/m}^2$ with $R_f = 10 \mu\text{m}$, $\bar{\varepsilon}_x = 0.4\%$

Estimation of $\Delta\theta_{max}$

$21 \times 1 - free$



$21 \times 1 - 1 \cdot t_{90^\circ}$



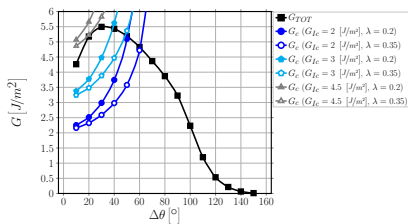
$$\Delta\theta_{max} \in (30^\circ - 105^\circ)$$

$$\Delta\theta_{max} \in (30^\circ - 50^\circ)$$

$$G_{TOT}(\Delta\theta) > G_c = G_{lc} \left(1 + \tan^2((1-\lambda)\Psi_G) \right), \quad \Psi_G = \tan^{-1} \left(\sqrt{\frac{G_{II}}{G_I}} \right) \Big|_{\Delta\theta}$$

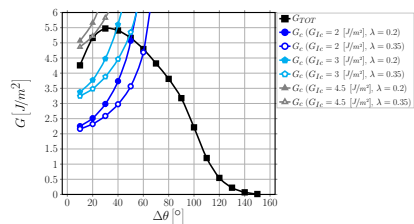
Estimation of $\Delta\theta_{max}$

$21 \times 3 - free$



$$\Delta\theta_{max} \in (40^\circ - 60^\circ)$$

$21 \times 3 - 1 \cdot t_{90^\circ}$

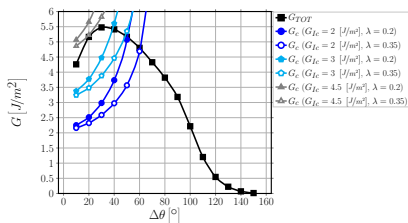


$$\Delta\theta_{max} \in (40^\circ - 60^\circ)$$

$$G_{TOT}(\Delta\theta) > G_c = G_{lc} \left(1 + \tan^2((1-\lambda)\Psi_G) \right), \quad \Psi_G = \tan^{-1} \left(\sqrt{\frac{G_{II}}{G_I}} \right) \Big|_{\Delta\theta}$$

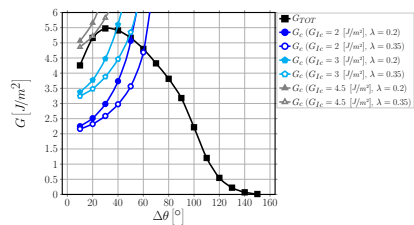
Estimation of $\Delta\theta_{max}$

$21 \times 21 - free$



$$\Delta\theta_{max} \in (40^\circ - 60^\circ)$$

$21 \times 21 - 1 \cdot t_{90^\circ}$

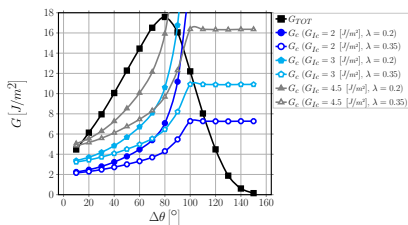


$$\Delta\theta_{max} \in (40^\circ - 60^\circ)$$

$$G_{TOT}(\Delta\theta) > G_c = G_{lc} \left(1 + \tan^2((1-\lambda)\Psi_G) \right), \quad \Psi_G = \tan^{-1} \left(\sqrt{\frac{G_{II}}{G_I}} \right) \Big|_{\Delta\theta}$$

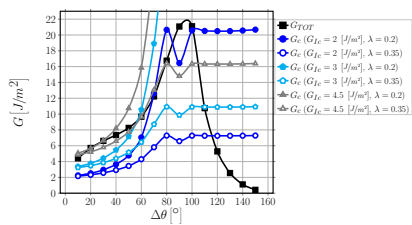
Estimation of $\Delta\theta_{max}$

$21 \times 21 - symm$



$$\Delta\theta_{max} \in (80^\circ - 110^\circ)$$

$21 \times 21 - asymm$



$$\Delta\theta_{max} \in (55^\circ - 115^\circ)$$

$$G_{TOT}(\Delta\theta) > G_c = G_{lc} \left(1 + \tan^2((1-\lambda)\Psi_G) \right), \quad \Psi_G = \tan^{-1} \left(\sqrt{\frac{G_{ll}}{G_l}} \right) \Big|_{\Delta\theta}$$

Comparison with Experimental Observations (literature)

Estimated debond size range in cross-ply ($n \times k - 1 \cdot t_{90^\circ}$)

$40^\circ - 60^\circ$

Measured debond size range in cross-ply (Correa et al., Compos. Sci. Technol. 155 (213-220), 2018)

$21.4^\circ - 89.2^\circ$, average 49.3° , standard deviation of 11.7°

63% of measurements in $40^\circ - 60^\circ$ range

 **MOVING FORWARD**

Moving Forward: Ideas

- ▶ Microscopic characterization of transverse cracks, debonds and microstructure: optical microscope and image analysis, edge view (both sides), increasing load levels on same specimen, different lay-ups and materials
 - SEM? TEM? μ -CT?
- ▶ Microstructure-controlled debonding as toughening mechanisms for thin-ply laminates
 - 3D-printing? Improved spread-tow technique?

Thank you for listening today!



LULEÅ
UNIVERSITY
OF TECHNOLOGY



Education and Culture

Erasmus Mundus